Communications in Computational Chemistry
Commun. Comput. Chem., Vol. 7, No. 2, 111–119
doi: 10.4208/cicc.2025.80.01
Regular Article

Unraveling the Impact of Non-Covalent Interactions and Different Donor Moieties on Charge Transport in DPPT-Based Polymers

Jinyang Luo[1], Jiawei Dong[2], Guo Wang[1], Linjun Wang[2,*] and Hua Geng[1,*]

[1]*Department of Chemistry, Capital Normal University, Beijing 100048, China;*

[2]*Zhejiang Key Laboratory of Excited-State Energy Conversion and Energy Storage, Department of Chemistry, Zhejiang University, Hangzhou 310058, China*

[*] Corresponding authors: ljwang@zju.edu.cn, hgeng@cnu.edu.cn

Received on 21 March 2025; Accepted on 23 April 2025

Abstract: The integration of both rigid and flexible components holds great potential to significantly enhance the overall performance of organic electronic devices. Non-covalent interactions are frequently harnessed to augment the planar conjugation of polymers, consequently elevating the rigidity of these polymers. However, the influence of the dihedral angle distortion between donor and acceptor units, which is induced by the flexibility inherent in donor-acceptor copolymers, on charge transport remains poorly understood. In this study, we systematically investigate intra-chain charge transport parameters and charge mobility for the 3,6-bis(thiophen-2-yl) diketopyrrolopyrrole (DPPT) conjugated with various donor moieties. Combining with density functional theory (DFT) and the Su-Schrieffer-Heeger (SSH) model, we find that when the non-covalent interactions between the donor and acceptor units are enhanced (as exemplified by DPPT-FT and DPPT-BO), the coupling between electrons and low-frequency vibrations is significantly suppressed. Simultaneously, the intra-chain electronic coupling increases owing to substantial orbital overlap. Surface hopping simulations are utilized to study the charge transport properties. For DPPT-T, DPPT-FT, and DPPT-BT, weaker molecular rigidity and disordered chain packing lead to thermally activated hopping transport (low electronic coupling and high reorganization energy). In contrast, the enhanced structural rigidity of DPPT-BO facilitates charge delocalization, leading to an initial improvement in carrier mobility under low-temperature conditions, and thermal fluctuation effects induce a band-like behavior at high temperature.

Key words: charge transport, Diketopyrrolopyrrole copolymers, torsional stiffness, non-covalent interactions, Su-Schrieffer-Heeger model.

1. Introduction

Conjugated donor-acceptor (D-A) polymers as organic semiconductor materials have attracted much attention due to their promising applications in organic electronic devices [1,2]. The performance of these devices heavily depends on the charge transport properties of the D-A conjugated polymers. For these kind of polymers, covalent interactions establish main-chain backbone, determining its fundamental charge transport capability, while non-covalent interactions (including hydrogen bonds, van der Waals forces, π-π stacking, electrostatic

interactions, etc.) modify the backbone, regulating intra-chain and inter-chain behavior as well as macroscopic properties (such as charge mobility and flexibility) [3-6]. With respect to inter-chain charge transport, it is more susceptible to the solvent used during device fabrication, the film preparation process, and the impact of side chains [6-8]. Intra-chain charge transport better reflects the intrinsic transport properties.[9-11] Through designing different donor-acceptor unit combinations within the polymer chain, remarkable high charge mobility has been obtained [11-14].

It is difficult to fully understand the influence of intra-chain non-covalent interactions on charge transport dynamics, since intra-chain non-covalent interactions have multiple impacts [4,6] [i] Intra-chain non-covalent interactions induce coplanar chain conformation, which facilitates π-orbital overlap, increases electronic coupling (V) and narrows the bandgap (E_g). The smaller Donor-Acceptor dihedral, the larger electronic coupling [15-17]. [ii] Intra-chain non-covalent interactions can restrict torsional freedom, promoting planar or folded conformations that minimize geometric disorder. By stabilizing chain geometry, intra-chain interactions decrease the reorganization energy (λ) required for charge transfer, enhancing the exponential term in Marcus theory [4]. [iii] Intra-chain non-covalent interactions can lower thermal activation barriers, enabling more efficient charge transport, especially at low temperatures [4,15]. However, excessively strong intra-chain interactions may create deep energy traps, capturing charge carriers, and increases trap density, reducing overall mobility [11, 12].

On the other hand, diketopyrrolopyrrole (DPP) based copolymers have attracted widely attention due to excellent ambipolar charge transport properties [1,18]. The measured values of charge mobility vary significantly under different experimental conditions. When DPPT, the derivative of DPP, is combined with different donor moieties, i.e., thiophene (T), 3,4-difluorothiophene (FT), benzothiadiazole (BT), benzooxadiazole (BO) then copolymerized, four D-A copolymers labeled as DPPT-T, DPPT-FT, DPPT-BT, DPPT-BO are obtained, the charge mobilities of these molecules range from 10^{-5} to 9.24 $cm^2V^{-1}s^{-1}$ under different experimental conditions [19-23]. But for the purpose of comparison, we select the results obtained under same device structure (in a bottom-gate top contact (BG-TC) with SiO_2 as the dielectric) [22,23], and their charge mobilities in organic thin-film transistors have been reported ranging from 10^{-5} to 0.64 $cm^2V^{-1}s^{-1}$(see **Scheme 1**).

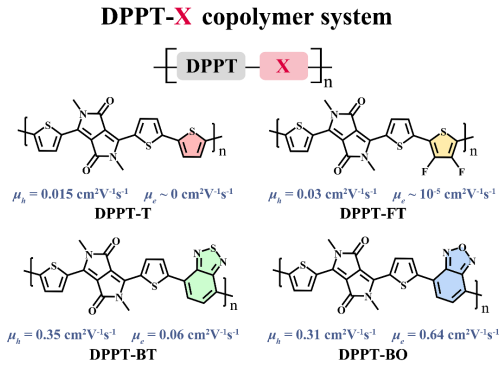

Scheme 1. Investigated systems for DPPT-T, DPPT-FT, DPPT-BT and DPPT-BO copolymers, μ_h (μ_e) is the experimentally measured hole (electron) mobility [22, 23].

To unravel the impact of non-covalent interactions and different donor moieties on charge transport in DPPT-based polymers, we constructed the molecular structures for the copolymers of DPPT-T, DPPT-FT, DPPT-BT, DPPT-BO, as seen in Scheme1. Based on charge transport parameters and the Su-Schrieffer-Heeger (SSH) model [24], we find that strengthening non-covalent interactions between donor and acceptor units markedly reduces the coupling between electrons and low-frequency vibrations. Simultaneously, intrachain electronic coupling is enhanced. As the rigidity of DPPT copolymers increases, charge mobility obtained by surface hopping simulation exhibits a steeper rise with temperature. This behavior suggests diminished energy loss from charge relaxation due to intramolecular vibrations, thereby promoting efficient intra-chain charge transport.

2. Theoretical methodology

To study charge transport properties and to calculate intra-chain electron and hole mobilities, the DPPT copolymers were coarse-grained as one-dimensional arrays of DPPT and X units, based on tight-binding Su-Schrieffer-Heeger model, which considers both local and non-local electron–phonon (e-ph) couplings.[24] Thus, the electronic structure of these polymers can be described by the following total Hamiltonian [10,25],

$$H = H_e + H_n \tag{1}$$

with the electronic part written as

$$\begin{aligned} H_e = & \sum_{k=1}^{N} \left(\epsilon_k + \alpha_{k,1}x_{k,1} + \alpha_{k,2}x_{k,2}\right) |k\rangle\langle k| \\ & + \sum_{k=2}^{N} J \left|cos\,\theta_{k,k-1}\right| \left[|k\rangle\langle k-1| + |k-1\rangle\langle k|\right] \end{aligned} \tag{2}$$

and the nuclear part as

$$\begin{aligned} H_n = & \sum_{k=1}^{N} \frac{1}{2}\begin{pmatrix} m_{k,1}v_{k,1}^2 + K_{k,1}x_{k,1}^2 + m_{k,2}v_{k,2}^2 \\ +K_{k,2}x_{k,2}^2 + I_k\omega_{k,3}^2 \end{pmatrix} \\ & + \sum_{k=2}^{N} \frac{K_\theta}{2}\left(\theta_{k,k-1} - \theta_{eq}\right)^2 \end{aligned} \tag{3}$$

Here, ϵ_k represents the on-site energy of the donor/acceptor moiety in the neutral ground-state equilibrium geometry. J is the electronic (hole or electron) coupling modulated by a cosine function with angle $\theta_{k,k-1}$ describing the torsion between the DPPT and X units.[10, 25] The nuclear dynamics is described by three effective, classical, harmonic vibrational degrees of freedom: $x_{k,1}$, $x_{k,2}$, and $\theta_{k,k-1}$. The first two represent a high- and low-frequency intra-monomer mode, respectively, and account for the change in monomer geometry upon addition of excess holes or electrons. The k-th monomer energy is linearly modulated with these parameters by a local electron-phonon coupling constant ($\alpha_{k,1}$ and $\alpha_{k,2}$). This, in turn, is related to the relaxation energy $\lambda_{k,1(2)}$ by $\alpha_{k,1} = \sqrt{2K_{k,1(2)}\lambda_{k,1(2)}}$. The force constant of the harmonic oscillator is $K_{k,1(2)} = m_{k,1(2)}\omega_{k,1(2)}^2$,

where $m_{k,1(2)}$ is the reduced mass of the monomer k, $v_{k,1(2)}$ and $\omega_{k,1(2)}$ correspond to the linear velocity and angular frequency, respectively.[10, 25, 26] K_θ is the torsional stiffness constant.[10] We fit the torsion potential well (between DPPT and X) within a simple harmonic oscillator approximation and this led to the torsional stiffness constants of K_θ. The moment of inertia was evaluated as $I_k = m_k R^2$, where the masses were taken to be reduced masses of the DPPT and X units, and R was evaluated by measuring the distance between the centers of mass for two randomly selected DPPT or X units from the axes of rotation. The Hamiltonian in **eq.1** gives a rough one-dimensional (1D) representation of a periodic copolymer with DPPT and X sites present in the same unit cell, both contributing their HOMOs (LUMOs) to hole (electron) transport.

3. Results and discussion

3.1 Geometry structure and electron-phonon coupling

To investigate the influence of different X units on the structure of DPPT-X copolymers, we first constructed 1D periodic chains of DPPT-X and optimized their structures at the PBE level using the VASP code [10,27]. The bond length (d) and dihedral (θ_{1D}) between the DPPT and X units are shown in **Figure 1 (a), (b)** and **Figure S1** (the positive direction of θ was defined as the out-of-plane torsion of X units). θ_{1D} of DPPT-FT and DPPT-BO were 0° and 0.02°, respectively. Compared with -24.55° of DPPT-T and 14.51° of DPPT-BT, the molecular structures of DPPT-FT and DPPT-BO were more planar.

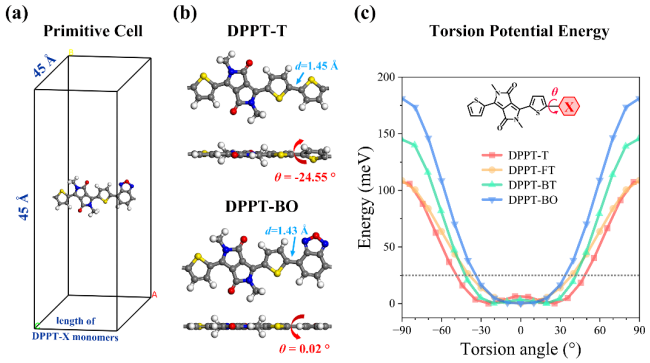

Figure 1. (a) Primitive cell (taking DPPT-BO for an example). (b) Front and side views of the DPPT-X monomer structures in the primitive cell of the 1D periodic chain (optimized at PBE level using VASP code). (c) Calculated torsion potential energy between DPPT and X units (at LRC-ωB97X-D/6-31g(d) level.

Furthermore, we performed a relaxed scan at various θ on the DPPT-X monomer (see **Figure 1 (c)**) at the LRC-ωB97X-D/6-31g(d) level [28], based on their optimized ground-state structures. For the DPPT-FT monomer, the range of the torsion angle when the torsional potential was lower than 25 meV extended from -40.00° to 40.00°, which had a narrower distribution compared to that of DPPT-T (-48.89° to 48.89°). Similarly, the DPPT-BO monomer exhibited a torsion angle range of -34.42° to 34.42° under the same torsional potential threshold, which was narrower than that of DPPT-BT (-44.59° to 44.59°). These θ_{eq} values are generally consistent with the equilibrium angle (θ_{1D}) obtained from 1D periodic chains (optimized at the PBE level using VASP code), which confirms the stability of these values. Then, we obtained the equilibrium torsion angle θ_{eq} and fit each potential well within a simple harmonic oscillator approximation and this led to torsional stiffness constants of K_θ, respectively.

Table 1. The torsional stiffness constant (K_θ) and equilibrium torsion angle (θ_{eq}) of each monomer.

Monomer	K_θ (cm^{-1}/rad^2)	θ_{eq} (°)
DPPT-T	842.14	±24.52
DPPT-FT	869.98	0
DPPT-BT	1251.41	±18.93
DPPT-BO	1540.19	0.03

As seen in **Table 1**, K_θ of DPPT-FT was 869.98 cm^{-1}/rad^2, which was higher than that of DPPT-T (842.14 cm^{-1}/rad^2), implying that DPPT-FT is relatively more rigid and more difficult to twist than DPPT-T, with its θ_{eq} being 0°. Meanwhile, K_θ of DPPT-BO was 1540.19 cm^{-1}/rad^2, higher than that of DPPT-BT (1251.41 cm^{-1}/rad^2), which indicates that DPPT-BO was relatively more rigid and harder to twist than DPPT-BT, with its θ_{eq} being 0.03°. Higher K_θ indicated that the intramolecular torsion became more difficult, the steric hindrance of torsion angle increased dramatically from DPPT-T, DPPT-FT, DPPT-BT and DPPT-BO.

To investigate the underlying mechanism of the rigidity of DPPT-FT and DPPT-BO, we performed a natural bond orbital (NBO) analysis on the DPPT-X monomers (based on the molecular structures at the minimum energy points) to obtain the variation of energy ($E^{(2)}$) and compare the non-covalent interaction between DPPT and X units [4, 29-31].

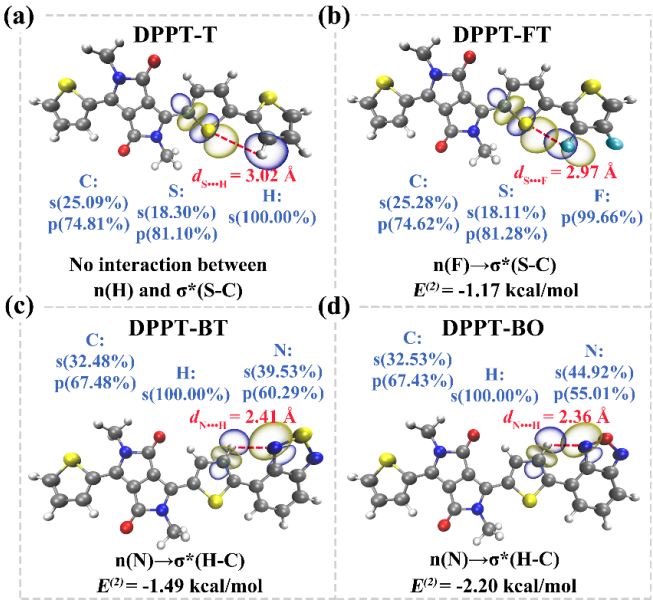

Figure 2. Non-covalent interactions between DPPT and X units: NBO overlap between the n-orbital and the σ*-orbital, in which the percentage represents the contribution of atomic orbitals participating in hybridization, and the orbital interaction energy $E^{(2)}$ (at LRC-ωB97X-D/6-31g(d) level).

As shown in **Figures 2 (a), (b)**, for DPPT-T, the overlap between n(H) and σ*(S-C) orbitals was negligibly small. However, for DPPT-FT, the distance between sulfur and fluorine atoms was 2.97 Å. Additionally, the $E^{(2)}$ value of the n(F)→σ*(S-C) interaction was -1.17 kcal/mol, aligning with the category of chalcogen bond [32-34]. This weak interaction between DPPT and FT fixed their torsion angle

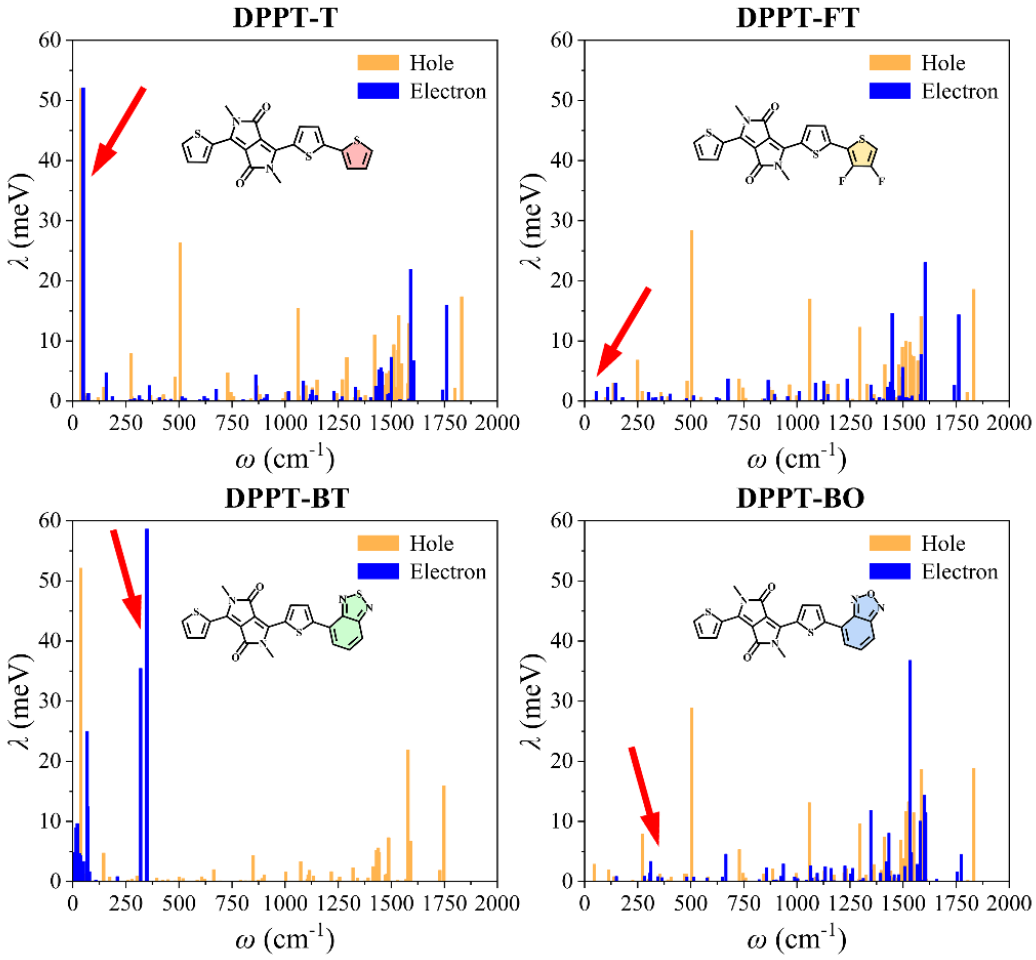

Figure 3. Reorganization energies (λ) for the four investigated DPPT-X monomers.

at 0°. As for DPPT-BO, the distance between nitrogen and hydrogen atoms in DPPT-BO ($d_{N\cdots H}$ = 2.36 Å) was shorter than that in DPPT-BT ($d_{N\cdots H}$ = 2.41 Å). Meanwhile, the $E^{(2)}$ value of the n(N)→σ*(H-C) interaction is -2.20 kcal/mol, which was lower than that of DPPT-BT (-1.49 kcal/mol), aligning with hydrogen bond interactions [35]. Consequently, the stronger weak interaction between DPPT and BO stabilized their torsion angle near 0°, as shown in **Figures 2 (c), (d).**

Furthermore, local electron-phonon couplings are connected to the polaron relaxation energies induced by the excess hole (electron) present on the polymer. To calculate these terms, we investigated the relaxation energy of DPPT-X monomers based on their optimized geometry structure for ground state and charged (i.e., anionic or cationic) state at the LRC-ωB97X-D/6-31g(d) level. We projected each intra-molecular normal mode of vibration on the vector describing the geometric changes between the neutral and charged states to partition the relaxation energies into mode contributions, utilizing the MOMAP software package [36,37]. Based on the harmonic-oscillator approximation, the total reorganization energies (λ) may be partitioned into contributions from each vibrational mode (see **Figure 3**) [26,36,37]. As for DPPT-FT in both cationic and anionic states, the vibrations were suppressed at low frequencies (especially the vibrational mode at ω = 43.44 cm⁻¹) , compared with DPPT-T. And λ_h of DPPT-FT was 214.57 meV, λ_e was 121.33 meV, both of which were slightly lower than those of DPPT-T (λ_h = 272.83 meV, λ_e = 168.94 meV). Compared with DPPT-BT, the vibrations of DPPT-BO in anionic state were significantly suppressed at low frequencies (especially the vibrational mode at ω = 342.94 cm⁻¹), thus λ_e of DPPT-BO was 160.85 meV, which was lower than that of DPPT-BT (λ_e = 230.35 meV). However, in the cationic state, the relaxation energies of DPPT-BO at low frequencies were slightly higher than those of DPPT-BT. Therefore, λ_h of DPPT-BO was 201.97 meV, which was slightly higher than that of DPPT-BT (λ_h = 168.81 meV).

3.2 Band structure and electronic coupling

We then calculated the band structure (see **Figure 4**) and further obtained the electronic coupling J_h (J_e) between the HOMO (LUMO) orbitals of the DPPT and X units for hole (electron) (at the PBE level using VASP code) [10,27]. We used the DPPT-X minimal representation to describe the two highest occupied valence bands (i.e., VB and VB-1) and the two lowest unoccupied conduction bands (i.e., CB and CB+1) of DPPT-X copolymer and provided the values for the parameters ϵ_k and J. The geometric structure of the 1D periodic polymer chains were optimized at the PBE level using VASP code [27]. Uniform 21×1×1 Monkhorst-Pack k-point mesh was employed for all DPPT-X copolymers.

In **Table 2**, we presented the properties of band structure and electronic couplings of the studied DPPT-X systems. DPPT-BT and DPPT-BO exhibited smaller bandgaps (0.45 eV and 0.32 eV, respectively) compared to DPPT-T (0.82 eV) and DPPT-FT (0.83 eV), which was favorable for electron injection. The electronic couplings at equilibrium torsion angles (J_h^{eq} and J_e^{eq}) showed distinct trends: DPPT-T had the highest electronic coupling (363.74 meV) despite its large bandgap, while the electronic coupling of DPPT-FT (362.85 meV) was nearly identical to that of DPPT-T but limited by its largest bandgap. The smaller bandgap of DPPT-BT was offset by its lowest electronic coupling (326.80 meV) and narrowest conduction band (0.42 eV), potentially restricting electron transport. In contrast, DPPT-BO combined the smallest bandgap with the highest hole electronic coupling (366.01 meV) and the largest valence band width (0.51 eV), indicating efficient hole delocalization. This suggested that its molecular structure promoted efficient hole delocalization.

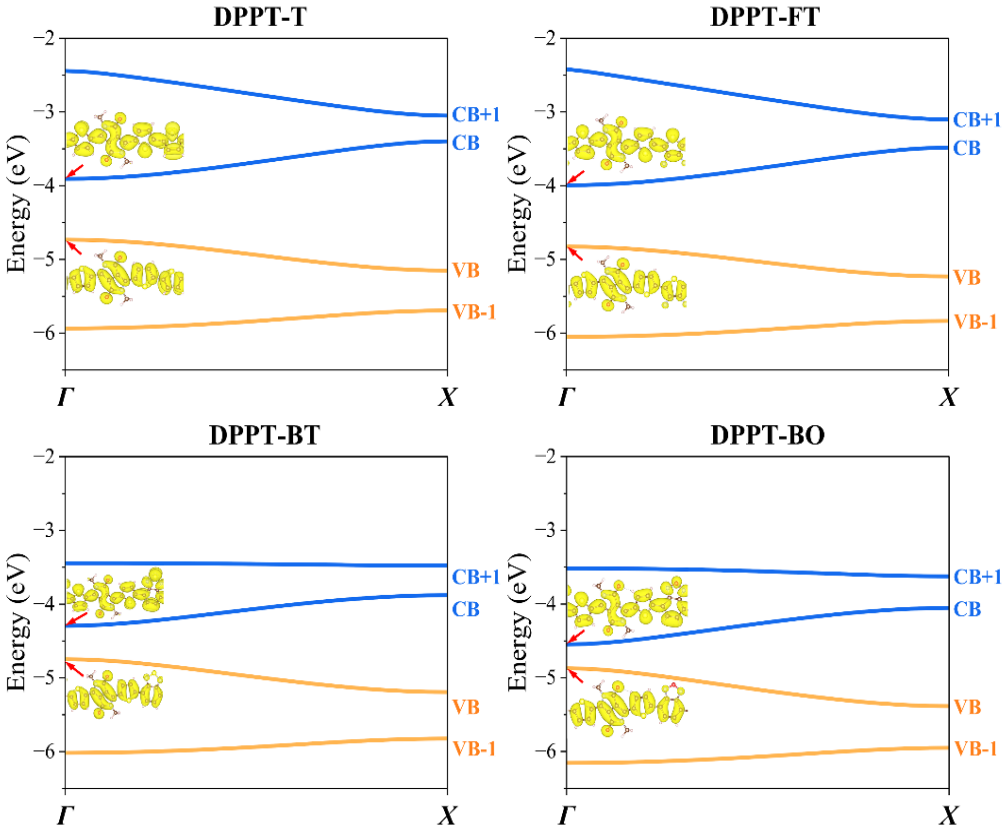

Figure 4. Band structure along the backbone direction (Γ-X (1,0,0)π/a) for the four investigated DPPT-X systems at equilibrium torsion angles (θ_{1D}).

Table 2. Properties of band structure and electronic couplings of 1D periodic chains.

System	E_{VB}[a] (eV)	E_{CB}[b] (eV)	E_{gap}[c] (eV)	W_{VB}[d] (eV)	W_{CB}[e] (eV)	J_h^{eq}[f] (meV)	J_e^{eq}[g] (meV)	θ_{1D}[h] (°)
DPPT-T	-4.74	-3.91	0.82	0.42	0.51	325.34	363.74	-24.55
DPPT-FT	-4.83	-4.00	0.83	0.40	0.51	319.32	362.85	0
DPPT-BT	-4.75	-4.30	0.45	0.45	0.42	337.51	326.80	14.51
DPPT-BO	-4.87	-4.55	0.32	0.51	0.50	366.01	360.17	0.02

[a], [b]The energy of the highest occupied valence band and the lowest unoccupied conduction band. [c]Band gap. [d], [e]Bandwidths of the valence band and conduction band. [f], [g]Electronic couplings for hole and electron when the torsion angles (θ) between DPPT and X units were at equilibrium. [h]Equilibrium torsion angles in 1D periodic chains (θ_{1D}).

Table 3. The difference in the changes of hole (ΔJ_h) and electron (ΔJ_e) coupling corresponding to θ when the torsional potential is lower than -25 meV.

System	ΔJ_h (meV)	ΔJ_e (meV)
DPPT-T	132.45	146.96
DPPT-FT	26.50	30.03
DPPT-BT	30.47	26.86
DPPT-BO	49.61	46.36

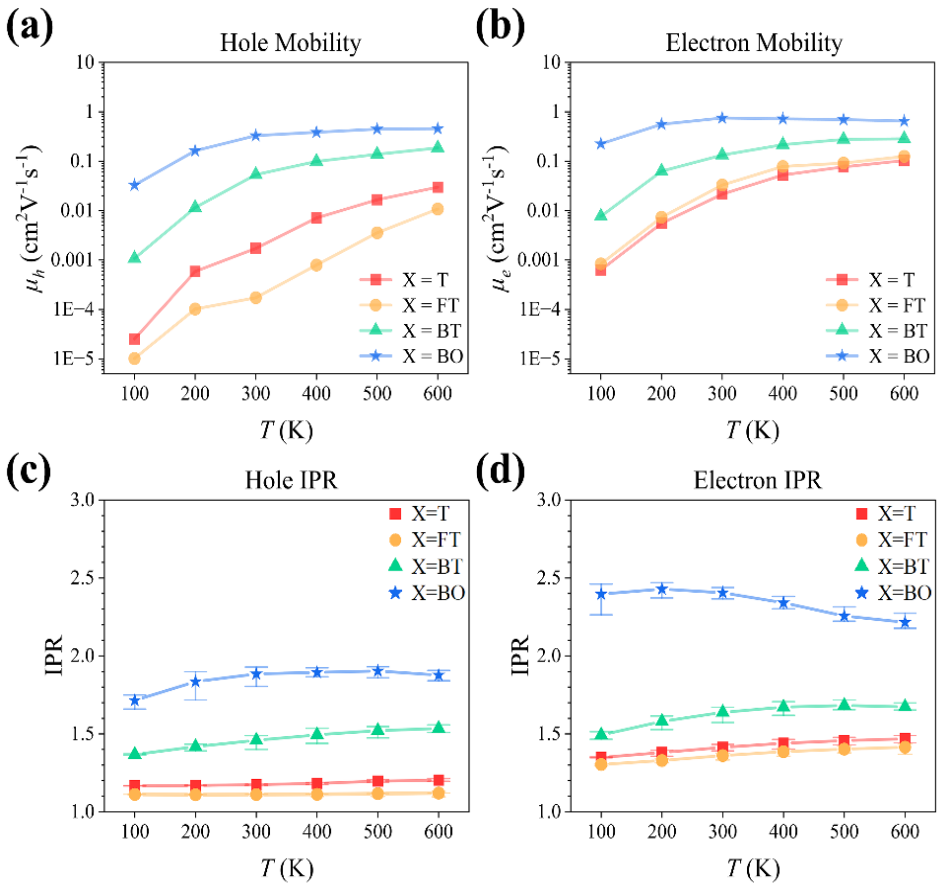

Figure 5. Temperature-dependent theoretical hole and electron transfer properties: (a), (b) mobility and (c), (d) related IPR for the four investigated DPPT-X copolymers.

It was shown in **Table 3** that ΔJ_h (132.45 meV) and ΔJ_e (146.96 meV) of DPPT-T were both higher than those of DPPT-FT (meV and 30.03 meV, respectively), indicating that the symmetric backbone structure of DPPT-T was more sensitive to conformational fluctuations at low torsional potentials. However, both ΔJ_h (49.61 meV) and ΔJ_e (46.36 meV) of DPPT-BO were larger than those of DPPT-BT (30.47 meV and 26.86 meV, respectively), suggesting that its planar equilibrium structure experienced greater coupling fluctuations under low torsional potentials. Notably, the strongest non-covalent interactions within DPPT-BO monomers endowed it with the highest rigidity, which stabilized its hole and electron couplings closer to the values under planar conformations. These results demonstrated that optimizing conformational stability through backbone design was critical for maximizing the charge transport efficiency.

3.3 Charge mobility simulation

The charge transport simulation was carried out using the Simulation Package for non-Adiabatic Dynamics in Extended systems (SPADE) [38], which supports the use of arbitrary function forms to construct the diabatic Hamiltonian and the state-of-the-art crossing corrected surface hopping methods to study large-scale nonadiabatic dynamics [10,39-42]. Based on the SSH model described above, we constructed one-dimensional chains of DPPT-X copolymers, each copolymer chain contained 21 sites, where each site corresponds to a DPPT-X repeat unit. For each DPPT-X site, a single hole state (electron state) was considered. For each simulation, the time-step size was set to be 1 fs, and the total simulation time was 2000 fs. The total number of surface hopping trajectories was set to 2000 to obtain a liner time evolution profile of mean squared displacement MSD(t) (see **Figure S9-S10**), via linear fitting of MSD(t) and the Einstein relation, we calculated the hole and electron mobility.

As shown in **Figure 5**, from DPPT-T to DPPT-BO, as the rigidity gradually increased, the hole mobility changed from 1.72×10^{-3} to 3.30×10^{-1} cm^{2}V^{-1}s^{-1}, and the electron mobility changed from 2.15×10^{-2} to 7.48×10^{-1} cm^{2}V^{-1}s^{-1} (at 300K). A contributing factor to this trend was the lower reorganization energies (both hole and electron) for BT/BO relative to T/FT (see **Figure S6** and **Table S4**). Notably, DPPT-BO exhibited the highest electron and hole mobilities, which could be attributed to its large electronic coupling and relatively small reorganization energy of BO. From DPPT-T to DPPT-BO, the theoretically calculated mobility presents an increasing trend, which is qualitatively consistent with experimental OFET measured charge mobility [22,23]. However, quantitative discrepancies between theoretical predictions and experimental data still exist. The impact of inter-chain packing, and the long alkyl side chains with significant steric hindrance, which may have a considerable impact on charge transport parameters, such as inter-chain electronic coupling, torsional stiffness constant (K_θ). We have tested hole and electron MSD and motilities (μ_h and μ_e) of DPPT-BO copolymer at different K_θ values under 300 K, (see **Table S7**). As the K_θ value increased, the motilities were enhanced. In addition, we treat the D -A unit as a site and thereby ignore super-exchange effect on charge transport. And thus, Theoretical

predictions of charge mobility underestimate the charge mobility of actual polymer materials.

The DPPT-X systems exhibited significant temperature-dependent transport characteristics (see **Figure 5**). In the low-temperature region (100–300 K), the hopping mode dominated. With respect to DPPT-T, DPPT-FT and DPPT-BT, the IPR values of holes and electrons are approximately 1.0 to 1.5 at low temperatures, indicating that the hole wave functions could, on average, extend to 1~2 sites, i.e., 1~2 DPPT-X repeat units, presenting much localized character due to relatively small electronic coupling and large reorganization. With temperature increasing, showing a slight increasing trend, which is characteristic of the typical thermally activated hopping mechanism.

For DPPT-BO, the IPR values of holes ranged from 1.71 to 1.88, indicating that the hole wave functions could, on average, extend to 1~2 sites; the IPR values of electrons ranged from 2.40 to 2.43, indicating that the electron wave functions could, on average, extend to 2~3 sites. Here, each site represents a DPPT-BO repeat unit. This was because DPPT-BO had the largest hole couplings and the lowest reorganization energy, which facilitated hole delocalization. Therefore, it had the highest IPR values for hole. Since the electron couplings of DPPT-BO were not significantly different from that of other copolymers, but its reorganization energy was relatively lower, its IPR values for electron were also quite high. Thus, both its hole and electron mobilities were significantly higher than those of the other copolymers. However, under high temperature larger than 300K, due to the torsional changes in the dihedral angle between donor and acceptor, thermal fluctuations in electronic coupling are induced, leading to the localization of wave functions. Consequently, the IPR exhibits a decreasing trend with increasing temperature, resulting in band-like transport behavior in the high temperature range for DPPT-BO copolymer.

To summarize, as for DPPT-T, DPPT-FT, and DPPT-BT, the intramolecular non-covalent interactions and the molecular rigidity are relatively weak, and thus the intra-chain structure of polymer chains exhibits a relatively disordered arrangement. Small electronic coupling and large reorganization energy induce a typical thermally activated hopping mechanism. While the DPPT-BO copolymer exhibits a relatively complex temperature-dependent mobility behavior due to its pronounced charge delocalization characteristics at low temperatures. The charge mobility rapidly reaches its maximum value and subsequently decreases with further temperature increase. Different temperature-dependent charge mobility essentially stems from the regulation of the structural rigidity, electronic coupling strength, and charge localization degree by different copolymer units (X) in DPPT.

4. Conclusion

This work has elucidated the critical roles of backbone rigidity and electronic coupling in governing the intra-chain charge transport properties of DPP-based copolymers. By comparing DPPT-T, DPPT-FT, DPPT-BT, and DPPT-BO systems, we have demonstrated that the enhancement of non-covalent interactions between the donor and acceptor structural units restricts the intra-molecular torsion. Moreover, rigid structures (such as DPPT-FT and DPPT-BO) possess higher torsional stiffness (K_θ), which suppresses structural disorder and reduces reorganization energies (λ) by up to 30% compared to their less rigid counterparts. Enhanced electronic couplings (J) in coplanar configurations further promote delocalized charge transport. These synergistic effects result in a remarkable increase in electron mobility and hole mobility for DPPT-BO. For DPPT-T, DPPT-FT, and DPPT-BT, weaker molecular rigidity and disordered chain packing lead to thermally activated hopping transport (low electronic coupling and high reorganization energy). In contrast, DPPT-BO's enhanced structural rigidity promotes charge delocalization at low temperatures, initially boosting mobility before thermal disorder dominates at higher temperatures. Our findings highlight that maximizing backbone rigidity and electronic coupling through strategic copolymer unit selection is a viable pathway to achieve high-performance organic semiconductors. This study not only advances the mechanistic understanding of charge transport in conjugated polymers but also offers actionable guidelines for molecular design targeting next-generation flexible electronics. Since the simplified charge transport model, we have underestimated charge mobility compared with the experimental measured results. In future work, we will further consider super-exchange effect, the steric hindrance of long alkyl side chains, the impact of intermolecular π-π stacking on charge transport parameters such as intra-chain torsion, inter-chain electronic coupling and low-frequency vibrations.

Supporting information

The online version contains supplementary material available at website.

https://global-sci.com/storage/self-storage/cicc-2025-80-1-r1-si.pdf

Acknowledgements

This work was supported by the National Natural Science Foundation of China (Grant Nos. 22273062, 22090022 and 22273082), the Beijing Municipal Natural Science Foundation (Grant No. 2192013), and the Open Project Fund of National Facility for Translational Medicine (Shanghai) (Grant No. TMSK-2024-109).

References

[1] Cheon H.J., An T.K., Kim Y.-H. Diketopyrrolopyrrole (DPP)-based polymers and their organic field-effect transistor applications: a review. *Macromol. Res.*, **30** (2022), 71-84.

[2] Yao Z.-F., Wang J.-Y., Pei J. Controlling morphology and microstructure of conjugated polymers via solution-state aggregation. *Prog. Polym. Sci.*, **136** (2023), 101626.

[3] Liu Y., Lu Y., Ding L., Pan C.K., Xu Y.C., Wang T.Y., Wang J.Y., Pei J. Fine-tuning the backbone conformation of conjugated polymers and the influence on solution aggregation and optoelectronic properties. *J. Polym. Sci.*, **61** (2023), 951-958.

[4] Liu M., Han X., Chen H., Peng Q., Huang H. A molecular descriptor of intramolecular noncovalent interaction for

regulating optoelectronic properties of organic semiconductors. *Nat. Commun.*, **14** (2023), 2500.

[5] Ji X., Cheng H.-W., Schuster N.J., LeCroy G.S., Zhang S., Wu Y., Michalek L., Nguyen B.-N.T., Chiong J.A., Schrock M., Tomo Y., Rech J., Salleo A., Gam S., Lee G.H., Tok J.B.H., Bao Z. Tuning the mobility of indacenodithiophene-based conjugated polymers via coplanar backbone engineering. *Chem. Mater.*, **36** (2023), 256-265.

[6] Mikie T., Okamoto K., Iwasaki Y., Koganezawa T., Sumiya M., Okamoto T., Osaka I. Naphthobispyrazine bisimide: a strong acceptor unit for conjugated polymers enabling highly coplanar backbone, short π–π stacking, and high electron transport. *Chem. Mater.*, **34** (2022), 2717-2729.

[7] Li Q.Y., Yao Z.F., Wu H.T., Luo L., Ding Y.F., Yang C.Y., Wang X.Y., Shen Z., Wang J.Y., Pei J. Regulation of high miscibility for efficient charge-transport in n-doped conjugated polymers. *Angew. Chem., Int. Ed.*, **61** (2022), e202200221.

[8] LeCroy G., Ghosh R., Sommerville P., Burke C., Makki H., Rozylowicz K., Cheng C., Weber M., Khelifi W., Stingelin N., Troisi A., Luscombe C., Spano F.C., Salleo A. Using molecular structure to tune intrachain and interchain charge transport in indacenodithiophene-based copolymers. *J. Am. Chem. Soc.*, **146** (2024), 21778-21790.

[9] Prodhan S., Qiu J., Ricci M., Roscioni O.M., Wang L., Beljonne D. Design rules to maximize charge-carrier mobility along conjugated polymer chains. *J. Phys. Chem. Lett.*, **11** (2020), 6519-6525.

[10] Carey R.L., Giannini S., Schott S., Lemaur V., Xiao M., Prodhan S., Wang L., Bovoloni M., Quarti C., Beljonne D., Sirringhaus H. Spin relaxation of electron and hole polarons in ambipolar conjugated polymers. *Nat. Commun.*, **15** (2024), 288.

[11] Pace G., Bargigia I., Noh Y.-Y., Silva C., Caironi M. Intrinsically distinct hole and electron transport in conjugated polymers controlled by intra and intermolecular interactions. *Nat. Commun.*, **10** (2019), 5226.

[12] Podzorov V. Long and winding polymeric roads. *Nat. Mater.*, **12** (2013), 947-948.

[13] Thomas T.H., Harkin D.J., Gillett A.J., Lemaur V., Nikolka M., Sadhanala A., Richter J.M., Armitage J., Chen H., McCulloch I., Menke S.M., Olivier Y., Beljonne D., Sirringhaus H. Short contacts between chains enhancing luminescence quantum yields and carrier mobilities in conjugated copolymers. *Nat. Commun.*, **10** (2019), 2614.

[14] Yao Z.F., Zheng Y.Q., Dou J.H., Lu Y., Ding Y.F., Ding L., Wang J.Y., Pei J. Approaching crystal structure and high electron mobility in conjugated polymer crystals. *Adv. Mater.*, **33** (2021), 2006794.

[15] Cheng C., Geng H., Yi Y., Shuai Z. Super-exchange-induced high performance charge transport in donor–acceptor copolymers. *J. Mater. Chem. C*, **5** (2017), 3247-3253.

[16] He F., Cheng C., Geng H., Yi Y., Shuai Z. Effect of donor length on electronic structures and charge transport polarity for DTDPP-based D–A copolymers: a computational study based on a super-exchange model. *J. Mater. Chem. A*, **6** (2018), 11985-11993.

[17] Zhang W.-N., Wu X.-Q., Wang G., Duan Y.-A., Geng H., Liao Y. Toward high performance ambipolar transport from super-exchange perspective: theoretical insights for IID-based copolymers. *Chin. J. Polym. Sci.*, **40** (2022), 355-364.

[18] Shen T., Jiang Z., Wang Y., Liu Y. Rational molecular design of diketopyrrolopyrrole-based n-type and ambipolar polymer semiconductors. *Chem. Eur. J.*, **30** (2024), e202401812.

[19] Bai J., Jiang Y., Wang Z., Sui Y., Deng Y., Han Y., Geng Y. Bar-coated organic thin-film transistors with reliable electron mobility approaching 10 $cm^2 V^{-1} s^{-1}$. *Adv. Electron. Mater.*, **6** (2019), 1901002.

[20] Wang Z., Shi Y., Deng Y., Han Y., Geng Y. Toward high mobility green solvent-processable conjugated polymers: a systematic study on chalcogen effect in poly(diketopyrrolopyrrole-alt-terchalcogenophene)s. *Adv. Funct. Mater.*, **31** (2021), 2104881.

[21] Wang Z., Gao M., He C., Shi W., Deng Y., Han Y., Ye L., Geng Y. Unraveling the molar mass dependence of shearing-induced aggregation structure of a high-mobility polymer semiconductor. *Adv. Mater.*, **34** (2022), 2108255.

[22] Homyak P., Liu Y., Liu F., Russel T.P., Coughlin E.B. Systematic variation of fluorinated diketopyrrolopyrrole low bandgap conjugated polymers: synthesis by direct arylation polymerization and characterization and performance in organic photovoltaics and organic field-effect transistors. *Macromol.*, **48** (2015), 6978-6986.

[23] Nodari D., Sharma S., Jia W., Marsh A.V., Lin Y.H., Fu Y., Lu X., Russkikh A., Harrison G.T., Fatayer S., Gasparini N., Heeney M., Panidi J. Conjugated polymer heteroatom engineering enables high detectivity symmetric ambipolar phototransistors. *Adv. Mater.*, **36** (2024), 2402568.

[24] Su W.P., Schrieffer J.R., Heeger A.J. Solitons in polyacetylene. *Phys. Rev. Lett.*, **42** (1979), 1698-1701.

[25] Dilmurat R., Prodhan S., Wang L., Beljonne D. Thermally activated intra-chain charge transport in high charge-carrier mobility copolymers. *J. Chem. Phys.*, **156** (2022), 084115.

[26] Troisi A. Prediction of the absolute charge mobility of molecular semiconductors: the case of rubrene. *Adv. Mater.*, **19** (2007), 2000-2004.

[27] Kresse G., Joubert D. From ultrasoft pseudopotentials to the projector augmented-wave method. *Phys. Rev. B*, **59** (1999), 1758-1775.

[28] Chai J.-D., Head-Gordon M. Long-range corrected hybrid density functionals with damped atom–atom dispersion corrections. *Phys. Chem. Chem. Phys.*, **10** (2008), 6615-6620.

[29] Reed A.E., Curtiss L.A., Weinhold F. Intermolecular interactions from a natural bond orbital, donor-acceptor viewpoint. *Chem. Rev.*, **88** (1988), 899-926.

[30] Hobza P. Calculations on noncovalent interactions and databases of benchmark interaction energies. *Acc. Chem. Res.*, **45** (2012), 663-672.

[31] Lu T., Chen F. Multiwfn: a multifunctional wavefunction analyzer. *J. Comput. Chem.*, **33** (2011), 580-592.

[32] Aakeroy C.B., Bryce D.L., Desiraju G.R., Frontera A., Legon A.C., Nicotra F., Rissanen K., Scheiner S., Terraneo G., Metrangolo P., Resnati G. Definition of the chalcogen bond (IUPAC Recommendations 2019). *Pure Appl. Chem.*, **91** (2019), 1889-1892.

[33] Politzer P., Murray J.S. Electrostatics and polarization in σ- and π-hole noncovalent interactions: an overview. *ChemPhysChem*, **21** (2020), 579-588.

[34] Clark T., Hennemann M., Murray J.S., Politzer P. Halogen bonding: the σ-hole. *J. Mol. Model.*, **13** (2007), 291-296.

[35] Grimme S. Semiempirical GGA-type density functional constructed with a long-range dispersion correction. *J. Comput. Chem.*, **27** (2006), 1787-1795.

[36] Shuai Z. Thermal vibration correlation function formalism for molecular excited state decay rates. *Chin. J. Chem.*, **38** (2020), 1223-1232.

[37] Reimers J.R. A practical method for the use of curvilinear coordinates in calculations of normal-mode-projected displacements and Duschinsky rotation matrices for large molecules. *J. Chem. Phys.*, **115** (2001), 9103-9109.

[38] Dong J., Qiu J., Bai X., Wang Z., Xiao B., Wang L. SPADE 1.0: a simulation package for non-adiabatic dynamics in extended systems. *J. Chem. Theory Comput.*, **21** (2025), 3300-3320.

[39] Wang L., Qiu J., Bai X., Xu J. Surface hopping methods for nonadiabatic dynamics in extended systems. *WIREs Comput. Mol. Sci.*, **10** (2019), e1435.

[40] Qiu J., Bai X., Wang L. Crossing classified and corrected fewest switches surface hopping. *J. Phys. Chem. Lett.*, **9** (2018), 4319-4325.

[41] Qiu J., Lu Y., Wang L. Multilayer subsystem surface hopping method for large-scale nonadiabatic dynamics simulation with hundreds of thousands of states. *J. Chem. Theory Comput.*, **18** (2022), 2803-2815.

[42] Tully J.C. Molecular dynamics with electronic transitions. *J. Chem. Phys.*, **93** (1990), 1061-1072.